Article

Homology-Based Interactions between Small RNAs and Their Targets Control Dominance Hierarchy of Male Determinant Alleles of Self-Incompatibility in *Arabidopsis lyrata*

Shinsuke Yasuda [1,†,‡]**, Risa Kobayashi** [1,‡]**, Toshiro Ito** [1]**, Yuko Wada** [1,*] **and Seiji Takayama** [2,*]

[1] Division of Biological Sciences, Nara Institute of Science and Technology, Nara 630-0192, Japan; shinsuke-yasuda@takii.co.jp (S.Y.); kobayashi.risa.ki7@bs.naist.jp (R.K.); itot@bs.naist.jp (T.I.)

[2] Department of Applied Biological Chemistry, Graduate School of Agricultural and Life Sciences, The University of Tokyo, Tokyo 113-8657, Japan

* Correspondence: yu-wada@gtc.naist.jp (Y.W.); a-taka@g.ecc.u-tokyo.ac.jp (S.T.)

† Present address: Plant Breeding and Experiment Station, Takii and Company, Limited, Konan, Shiga 520-3231, Japan.

‡ These authors contributed equally to this work.

Abstract: Self-incompatibility (SI) is conserved among members of the Brassicaceae plant family. This trait is controlled epigenetically by the dominance hierarchy of the male determinant alleles. We previously demonstrated that a single small RNA (sRNA) gene is sufficient to control the linear dominance hierarchy in *Brassica rapa* and proposed a model in which a homology-based interaction between sRNAs and target sites controls the complicated dominance hierarchy of male SI determinants. In *Arabidopsis halleri*, male dominance hierarchy is reported to have arisen from multiple networks of sRNA target gains and losses. Despite these findings, it remains unknown whether the molecular mechanism underlying the dominance hierarchy is conserved among Brassicaceae. Here, we identified sRNAs and their target sites that can explain the linear dominance hierarchy of *Arabidopsis lyrata*, a species closely related to *A. halleri*. We tested the model that we established in *Brassica* to explain the linear dominance hierarchy in *A. lyrata*. Our results suggest that the dominance hierarchy of *A. lyrata* is also controlled by a homology-based interaction between sRNAs and their targets.

Keywords: dominance hierarchy; self-incompatibility; epigenetics; small RNA; Brassicaceae; *Arabidopsis lyrata*

1. Introduction

Almost half of all angiosperms have a self-incompatibility (SI) system to avoid self-fertilization which helps maintain genetic diversity within the species. Most Brassicaceae plants, including *Arabidopsis lyrata*, have SI systems ensuring that the plants' sporophytic stigmas reject their own pollen grains. This SI reaction is genetically controlled by a single multiallelic locus called the *S* locus, which contains the pollen and stigma determinant genes *S-LOCUS PROTEIN 11* (*SP11*, also called *SCR*) [1–3] and *S-LOCUS RECEPTOR KINASE* (*SRK*) [4,5], respectively. The SI reaction in *Brassica rapa* is caused by the *S* haplotype-specific direct interaction between SP11 and SRK in the stigma epidermis [6,7]. These two genes are conserved in members of the Brassicaceae family, such as *Brassica oleracea* [4], *A. lyrata* [8], and *Arabidopsis halleri* [9].

B. rapa has a complicated dominance hierarchy among *SP11* alleles, which are expressed sporophytically in anther tapetum cells. Based on analysis of pollen phenotypes, class I (S_8, S_9, S_{52}, S_{12}) *SP11* alleles are dominant over class-II alleles (S_{44}, S_{60}, S_{40}, S_{29}) [10]. In addition, class-II alleles follow a linear dominance hierarchy: $S_{44} > S_{60} > S_{40} > S_{29}$ [10]. This complex hierarchy is controlled by interactions between just two sRNAs, *SP11 methylation inducer* (*Smi*) and *Smi2*, and their targets [11,12]. These sRNAs derive from inverted

repeat sequences and silence the relatively recessive *SP11* allele by inducing de novo DNA methylation of its promoter region [12,13]. *Smi* determines the dominance–recessivity relationships between class-I and class-II *SP11* alleles, and *Smi2* determines the linear relationships among the four class-II *SP11* alleles in a fashion dependent on the nucleotide sequences of the alleles. In particular, *Smi2* and its targets contain polymorphisms to control these complex linear relationships. Thus, we previously proposed a model in which interactions between sRNAs and targets based on sequence similarity control the complicated linear dominance hierarchy of male SI determinants [12].

Compared with cultivated *B. rapa*, *A. halleri*, a wild Brassicaceae species closely related to *Arabidopsis thaliana*, exhibits a more divergent hierarchical pollen dominance: $(S_{20, } S_{13}) > S_{12} > S_4 > S_3 > S_1$ [14]. A model describing how this male dominance hierarchy arose from multiple networks of sRNA target gains and losses has been proposed [9]. In addition, whether dominant *S* alleles carry a larger set of sRNAs, or whether a larger set of sRNA targets are carried by recessive *S* alleles, has been investigated [9].

A. lyrata also exhibits a complex pollen side dominance hierarchy among *S* haplotypes: class A2 $(S_{39}, S_{20}, S_{50}) >$ class A3 $(S_{13}, S_{16}) >$ class B $(S_{18}, S_{14}) >$ class A1 (S_1) [14–18]. However, the mechanism underlying this dominance hierarchy, including whether it involves sRNA(s), was unknown. Here, we identified sRNAs controlling the linear dominance hierarchy in *A. lyrata*, and we propose a homology-dependent model to explain the dominance–recessivity interaction of *SP11* in *A. lyrata*.

2. Results

2.1. Analysis of the Dominance–Recessivity Hierarchy of the SP11 Alleles

A. lyrata exhibits a male side dominance hierarchy of *S* haplotypes, comprising class A2 $(S_{39}, S_{20}, S_{50}) >$ class A3 $(S_{13}, S_{16}) >$ class B $(S_{18}, S_{14}) >$ class A1 (S_1) [14–18]. Here, for simplicity, we renamed these classes as follows: class IV $(S_{20}, S_{39}, S_{50}) >$ class III $(S_{13}, S_{16}) >$ class II $(S_{18}, S_{14}) >$ class I (S_1). We focused on the dominance–recessivity relationship between S_{20}-*SP11* (class IV) and S_{13}-*SP11* (class III) $(S_{20} > S_{13})$ because the only previously reported data about such relationships in *A. lyrata* pollen was that the expression of S_{13}-*SP11* is reduced in a $S_{20}S_{13}$ heterozygote, as revealed by gel blot analysis and in situ hybridization [19]. First, we analyzed *SP11* expression in anthers from both $S_{13}S_{13}$ homozygous and $S_{20}S_{13}$ heterozygous plants at different stages of development. Developing buds were divided into five stages based on size (Figure 1a). Reverse transcription quantitative real-time PCR (RT-qPCR) analysis showed that S_{13}-*SP11* transcripts started to accumulate at stage 2 (bud size: 1–2 mm) and showed maximum expression at stage 4 (bud size: 3–4 mm) in $S_{13}S_{13}$ homozygotes (Figure 1b). Similarly, in a previous study, RNA gel blot analysis revealed that *SP11* expression in *B. rapa* anthers reaches a maximum before flower opening, when tapetum cells are intact [3]. In contrast, we found that S_{13}-*SP11* transcript accumulation in $S_{20}S_{13}$ heterozygotes was strongly suppressed (to approximately 1%) compared with that in $S_{13}S_{13}$ homozygotes (Figure 1b), suggesting that S_{20}-*SP11* is dominant over S_{13}-*SP11.* This result is consistent with previously reported pollen phenotype data [14] and gel blot analysis of S_{13}-*SP11* in $S_{20}S_{13}$ heterozygotes [8]. Therefore, we focused on the molecular mechanism of the dominance–recessivity relationship among these *S* haplotypes.

2.2. Identification of sRNA and Its Precursor Genes in Class-IV S Haplotypes

To identify sRNA candidates controlling the dominance–recessivity relationships between S_{20}-*SP11* and S_{13}-*SP11*, we performed in silico analysis of the *S*-locus genomic sequences of the S_{20} haplotype. The aim was to identify sRNA candidate genes sharing high similarity with S_{13}-*SP11* between the region 500 base pairs (bp) upstream from its translational initiation site and 500 bp downstream from its termination codon. We identified an inverted repeat sequence that we named *Arabidopsis lyrata SMI1* (*AlSMI1*) (Figure 2a), which shares high similarity with the S_{13}-*SP11* intron region. *AlSMI1* is located 27.5 kbp downstream from S_{20}-*SP11* and approximately 37 kbp from S_{20}-*SRK*. We detected

inverted repeat sequences similar to that of S_{20}-*AlSMI1* in both the S_{39} and S_{50} haplotypes (class IV) (Figure 2a).
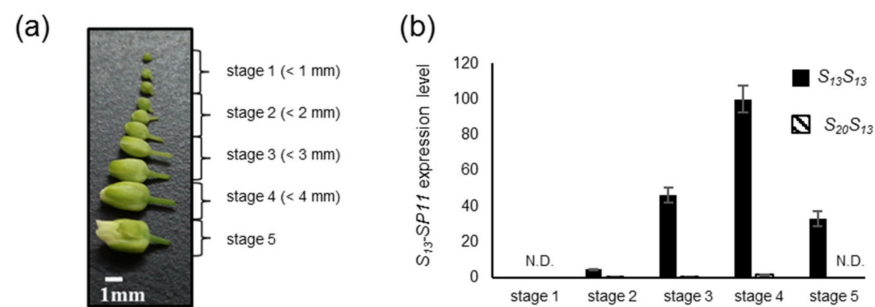

Figure 1. S_{13}-*SP11* expression in anthers during each stage of development and dominance–recessivity relationship between the S_{20} and S_{13} haplotypes. (**a**) Developmental stages of *Arabidopsis lyrata* anthers: stage 1, <1 mm; stage 2, <2 mm; stage 3, <3 mm; stage 4, <4 mm; stage 5, the day before flowering. (**b**) RT-qPCR analysis of S_{13}-*SP11* expression in $S_{13}S_{13}$ homozygotes and $S_{13}S_{20}$ heterozygotes. *Elf1α* was used as an endogenous reference gene. The results shown are means $\pm$ s.d. of 3 replicates. N.D., not detected.

We performed massively parallel sequencing to determine whether a 24-nucleotide (nt) sRNA is processed from S_{20}-*AlSMI1* prior to S_{13}-*SP11* expression. Since S_{13}-*SP11* expression begins at stage 2 (Figure 1b), we analyzed sRNA from stage 1 and 2 anthers of $S_{20}S_{13}$ heterozygotes and obtained 44,553,252 sRNA sequence reads. We identified 100 reads of the 24-nt sRNA *AlSmi1-a* (Figure 2b, Supplementary Table S1), which were processed from the S_{20}-*AlSMI1* precursor. RNAfold [20] predicted that S_{20}-*AlSMI1*, S_{39}-*AlSMI1*, and S_{50}-*AlSMI1* have hairpin-structured precursors (Figure 2c). We detected *AlSmi1-a* in the stem regions of S_{20}-*AlSMI1*, S_{50}-*AlSMI1*, and S_{39}-*AlSMI1* (Figure 2c; Supplementary Figure S1).

We also analyzed other *S*-locus genomic sequences of the S_{16} (class III), S_{14} and S_{18} (class II), and S_1 (class I) haplotypes, which are recessive to the S_{20} haplotype in the pollen dominance hierarchy. We searched the sequences of the S_{16}-, S_{18}-, S_{14}-, and S_1-*SP11* genes ±500 bp and determined that only the *AlSMI1-a* region in the *S* locus of the S_{20} haplotype shares high similarity with these *SP11* genes (Figure 2d; Supplementary Figures S1 and S2).

To evaluate the activity of *AlSmi1-a*, we calculated mispair scores [21] between the sRNA and S_{13}-*SP11*. Although the mispair score system was originally developed to predict whether a 21-nt microRNA (miRNA) cuts its target, it also efficiently predicted the 24-nt *Smi* and *Smi2* targets [12]. Mispair scores represent the number of mismatches of the complementary sites between an sRNA and its target, thus, high complementarity between an sRNA and its target leads to a lower mispair score. In our previous study, the SI phenotypes were not observed in transgenic *B. rapa* plants expressing *Smi/Smi2* with high sequence similarity with their own *SP11* (mispair scores ≤ 5.5), exhibiting DNA methylation at *SP11* and its silencing [11,12]. On the other hand, transgenic *B. rapa* plants expressing *Smi2* showing low similarity with their own *SP11* (mispair scores ≥ 6.5), exhibited unchanged SI phenotypes [12]. Therefore, the mispair scores between dominant *Smi* or *Smi2* and the target sites of recessive *SP11* were ≤5.5. Here, S_{20}-*AlSmi1-a* had a mispair score of <3.0 against the class-III *SP11* intron, <2.0 against the class-II *SP11* intron, and 4.0 against the class-I *SP11* intron (Figure 2e; Supplementary Figure S2). Both S_{39}-*AlSmi1-a* and S_{50}-*AlSmi1-a* had mispair scores of <5.0 against the *SP11* intron regions of all recessive *S* haplotypes (Figure 2e; Supplementary Figure S2), suggesting that *AlSmi1-a* potentially targets *SP11* in all recessive *S* haplotypes with the same dominance relationship: class IV > (class III, class II, class I). On the other hand, although class-IV *S* haplotypes (S_{20}, S_{50}) had target sites for *AlSmi1-a* (Figure 2d, Supplementary Figure S2), all *AlSmi1-a* sequences had mispair scores > 7.0 against these target sites (Figure 2e; Supplementary Figure S2).
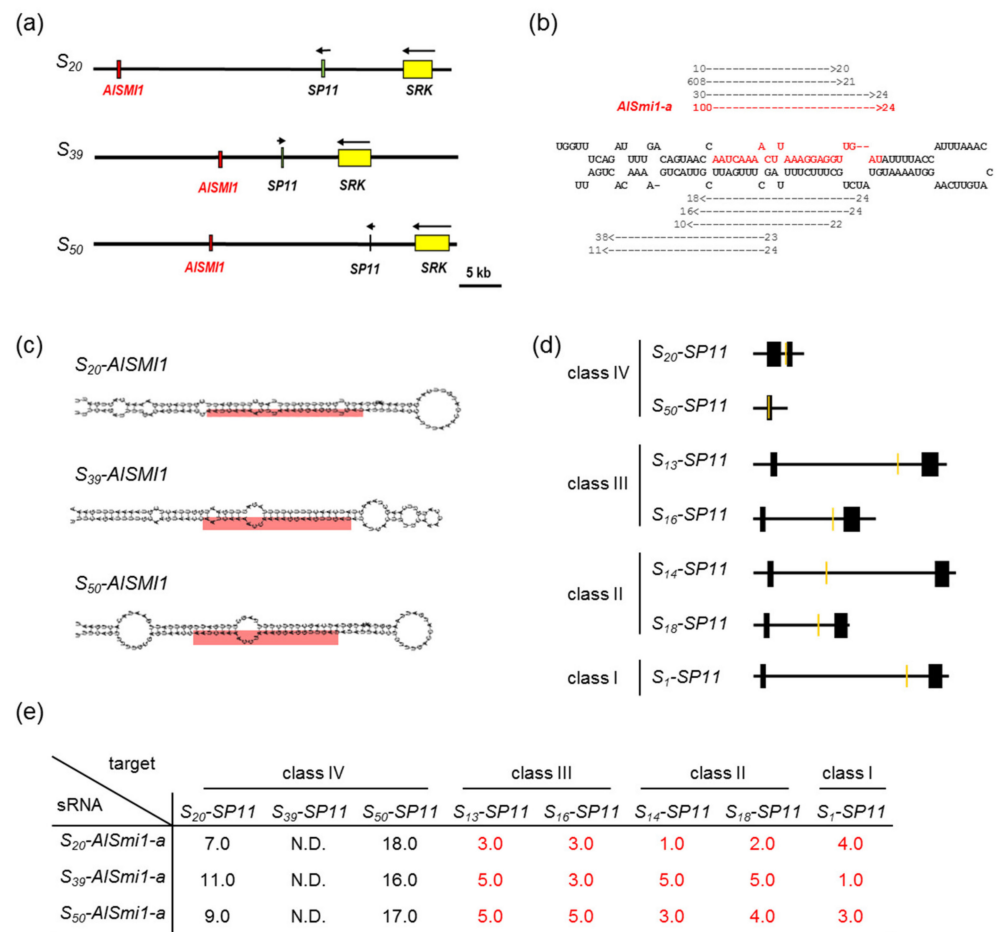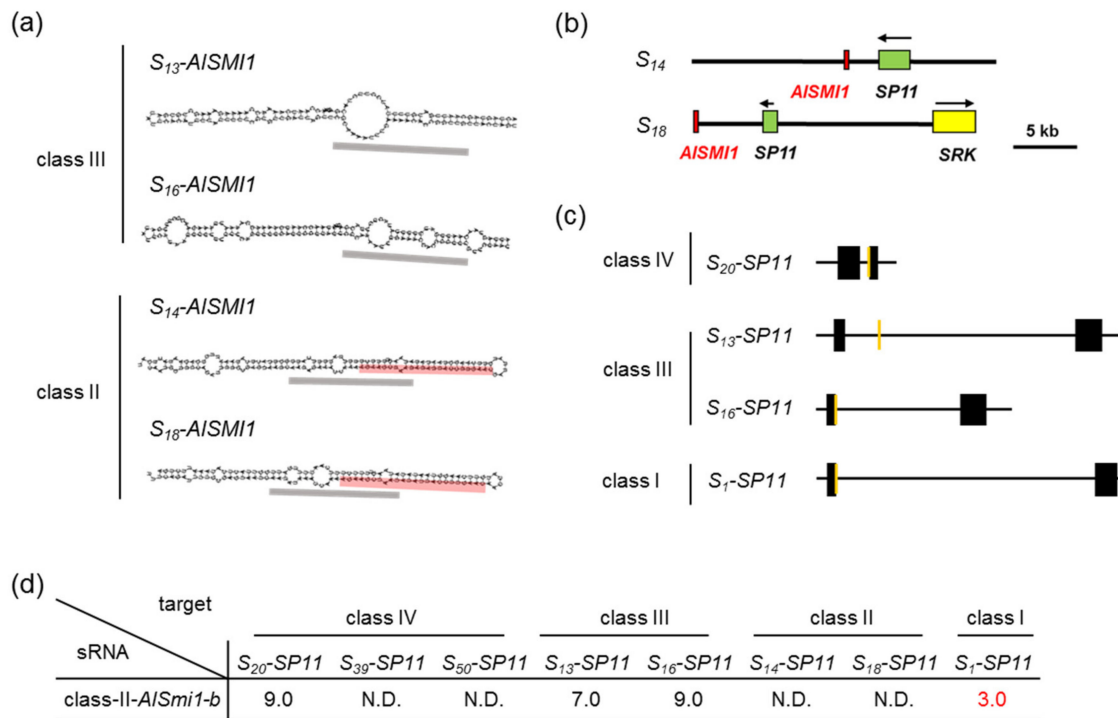
Figure 2. Identification of candidate sRNAs controlling the dominance–recessivity relationships: class IV > (class III, class II, class I). (**a**) Schematic diagrams of the *S* locus in the S_{20} haplotype (HQ379628), S_{39} haplotype (KJ772418–KJ772419), and S_{50} haplotype (HQ379631). Green, yellow, and red boxes indicate *SP11*, *SRK*, and *AlSMI1*, respectively. (**b**) Massively parallel sequencing analysis of sRNA expression from the *AlSMI1* inverted repeat sequence. sRNAs that obtained at least 10 reads were mapped against the *AlSMI1* inverted repeat sequence. Arrows indicate mapped sRNAs and their directions. Numbers at the tips of arrows indicate the number of obtained sRNA reads, and numbers at the ends of arrows indicate the length of each sRNA (in nucleotides). Bases in red represent the 24-nt *AlSmi1-a* region. (**c**) Stem-loop structures of *AlSMI1* of the S_{20}, S_{39}, and S_{50} haplotypes predicted by RNAfold [20]. The predicted mature 24-nt *AlSmi1-a* region is shown in red. (**d**) Schematic diagrams of the S_{20}, S_{50}, S_{13}, S_{16}, S_{14}, S_{18}, and S_1-*SP11* genomic regions. Black boxes indicate exon regions of *SP11* genes, orange boxes indicate regions with high sequence similarity to *AlSmi1-a*. (**e**) Sequence similarity between *AlSmi1-a* and *SP11*. Each number shows the mispair score between the class IV (S_{20}, S_{39}, S_{50})-*AlSmi1-a* and the *SP11* introns of class-IV, class-III, class-II, and class-I *S* haplotypes. N.D., not detected. Mispair scores < 5.5 are shown in red.

Based on these results, we suggest that *AlSmi1-a* is the only sRNA controlling the class IV > (class III, class II, class I) dominance hierarchy. On the other hand, *AlSMI1* genes are also conserved in class-III and class-II *S* locus with polymorphisms (Supplementary Figure S1).

2.3. Identification of sRNA and Its Precursor Genes in Class-II S Haplotypes

Next, we focused on the sequence polymorphisms of *AlSMI1* among class-III and class-II *S* haplotypes. *AlSMI1* genes from the S_{13} and S_{16} haplotypes (class III) and the S_{18} and S_{14} haplotypes (class II) have similar inverted repeat structures. However, the 24-nt S_{20}-*AlSmi1-a* sequence is not conserved among either class-III or class-II *S* haplotypes

(Figure 3a; Supplementary Figure S1). To analyze whether *AlSmi1* is processed in class-III *S* haplotypes, we mapped reads obtained by the massively parallel sequencing of $S_{20}S_{13}$ against the S_{13}-*AlSMI1* inverted repeat sequence. No reads were mapped onto the S_{13}-*AlSMI1* precursor. These results suggest that S_{13}-*AlSMI1* is not processed into 24-nt sRNAs and that *AlSMI1* is not functional in this class-III *S* haplotype (Figure 3a).
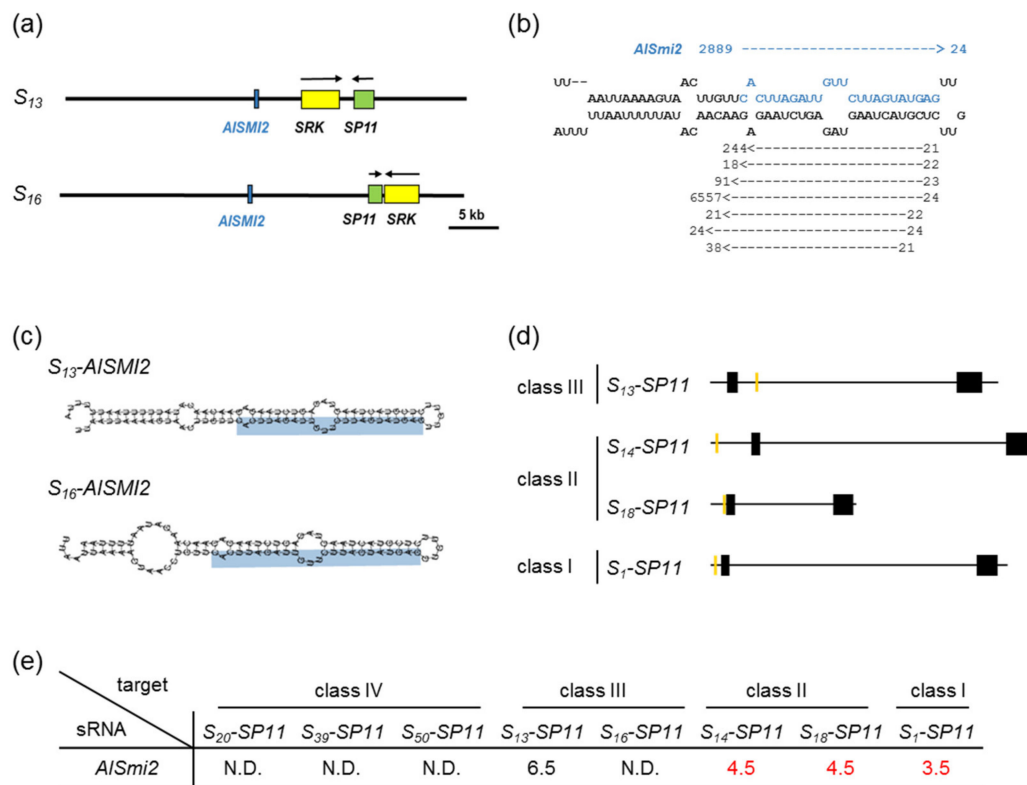

Figure 3. Identification of sRNAs controlling the dominance–recessivity relationships: class II > class I. (**a**) Stem-loop structures of the S_{13}, S_{16}, S_{14}, and S_{18} haplotypes of *AlSMI1* predicted by RNAfold [20]. Black dashed boxes indicate 24-nt snRNAs corresponding to class-III and class-II *AlSmi1-a*. The predicted 24-nt mature *AlSmi1-b* is shown in red. (**b**) Schematic diagrams of the *S* locus in the S_{14} haplotype (KJ772406) and S_{18} haplotype (KJ772412). Green, yellow, and red boxes indicate *SP11*, *SRK*, and *AlSMI1*, respectively. (**c**) Schematic diagrams of the *SP11* genomic regions of the S_{20}, S_{13}, S_{16}, and S_{1} haplotypes. Black boxes indicate exon regions of *SP11*, orange boxes indicate the target regions homologous to *AlSmi1-b*. (**d**) Sequence similarity between *AlSmi1-b* and *SP11*. Numbers are the mispair scores between class-II *AlSmi1-b* and class-IV, class-III, class-II, and class-I *S* haplotypes of *SP11*. N.D., not detected. Mispair scores < 5.5 are shown in red.

Interestingly, S_{18} and S_{14}-*AlSMI1* (class II) contain another 24-nt sequence (*AlSmi1-b*) that shares high similarity with a relatively recessive S_{1}-*SP11* (class I) exon junction (mispair score 3.0) (Figure 3a–d; Supplementary Figures S1 and S2). This suggests that sRNA processed from this region might be involved in the dominance relationship between class II and class I (class II > class I). *AlSmi1-b* had a mispair score > 7.0 against S_{20}-*SP11* (class IV) and S_{13}, S_{16}-*SP11* (class III), consistent with dominance hierarchy (class IV and class III > class II) (Figure 3c,d; Supplementary Figure S2). These results suggest that the interaction between *AlSmi1-a* from class-IV *S* haplotypes and its target site at the *SP11* intron of recessive class-III, class-II, and class-I *S* haplotypes controls the dominance relationships among these *S* haplotypes. On the other hand, the interaction between *AlSmi1-b* from class-II *S* haplotypes and its target site at the *SP11* exon junction of recessive class-I *S* haplotypes controls the dominance relationships among these *S* haplotypes.

2.4. Identification of sRNA and Its Precursor Genes in Class-III S Haplotypes

Since processed S_{13}-*AlSmi1* was not detected in $S_{20}S_{13}$ heterozygotes, we searched for other sRNAs that could control the dominance relationship class III > (class II and class I). We searched the *S* locus genomic sequence of the S_{13} haplotype, which shares high

similarity with class-II S_{14}- and S_{18}-SP11 and class-I S_1-SP11 genes ± 500 bp. We identified another inverted repeat sequence with high similarity to the 30-bp region upstream from the translation initiation sites of class-I and class-II *SP11* genes, which we named *A. lyrata SMI2* (*AlSMI2*) (Figure 4a). A database search identified the *AlSMI2* sequence only in the class-III S_{13} and S_{16} haplotypes (Figure 4a).

Figure 4. Identification of the candidate sRNAs controlling dominance–recessivity relationships: class III > (class II, class I). (**a**) Schematic diagrams of the *S* locus in the S_{13} haplotype (ADBK01001387) and the S_{16} haplotype (HQ379629). Green, yellow, and blue boxes indicate *SP11*, *SRK*, and *AlSMI2*, respectively. (**b**) Massively parallel sequencing analysis of sRNA expression from the S_{13}-*AlSMI2* inverted repeat sequence. sRNAs obtained from more than 10 reads were mapped against the S_{13}-*AlSMI2* inverted repeat sequence. Arrows indicate mapped sRNAs and their directions. Numbers at the tips of arrows indicate the obtained read numbers, and numbers at the ends of arrows indicate the base length of each sRNA. Bases in blue indicate the 24-nt *AlSmi2* region. (**c**) Stem-loop structures of *AlSMI2* of the S_{13} and S_{16} haplotypes predicted by RNAfold [20]. The predicted 24-nt mature *AlSmi2* is shown in blue. (**d**) Schematic diagrams of the *SP11* genomic regions of the S_{13}, S_{14}, S_{18}, and S_1 haplotypes. Black boxes indicate exon regions of *SP11*, orange boxes indicate the target region homologous to *AlSmi2*. (**e**) Sequence similarity between *AlSmi2* and *SP11*. Each number indicates the mispair score between class-III *AlSmi2* and class-IV, class-III, class-II, and class-I *S* haplotypes of *SP11*. N.D., not detected. Mispair scores < 5.5 are shown in red.

We mapped sRNA sequence reads derived from the anthers of $S_{20}S_{13}$ heterozygotes against the S_{13}-*AlSMI2* region and identified 2,889 *AlSmi2* reads sharing high similarity with the 5′ upstream region of *SP11* (Figure 4b; Supplementary Table S1). RNAfold [20] predicted that S_{13}-*AlSMI2* and S_{16}-*AlSMI2* had hairpin-structured precursors (Figure 4c). The mature 24-nt *AlSmi2* sequence was identified in the stem regions of S_{13}-*AlSMI2* and S_{16}-*AlSMI2* (Figure 4c).

AlSmi2 shares high similarity with the 5′ regions of the relatively recessive haplotypes S_{14}- and S_{18}-SP11 (class II) and S_1-SP11 (class I), with mispair scores < 4.5 (Figure 4d,e; Supplementary Figure S2). Although S_{13}-SP11 intron contains a candidate target site of *AlSmi2*, it showed low similarity with this sequence (mispair score 6.5) (Figure 4d,e; Supplementary Figure S2). These results suggest that *AlSmi2* controls the dominance

relationship class III > (class II, class I) as a result of its high similarity (mispair score < 4.5) with the *SP11* sequences of relatively recessive *S* haplotypes.

### 2.5. Quantification of a 24-nt sRNA and Its Precursor

To confirm the expression of S_{20}-*AlSMI1* and S_{13}-*AlSMI2*, which are precursors of S_{20}-*AlSmi1-a* and S_{13}-*AlSmi2*, respectively, in $S_{20}S_{13}$ heterozygotes, we performed RT-qPCR (Figure 5a). In *B. rapa*, the expression of *Smi1* and *Smi2* is induced before the initiation of *SP11* transcription [13]. Since *SP11* transcription is initiated at stage 2 in *A. lyrata* (Figure 1b), we analyzed S_{20}-*AlSMI1* and S_{13}-*AlSMI2* precursors in stage 1 and 2 anthers. We detected strong accumulation of both the S_{20}-*AlSMI1* and S_{13}-*AlSMI2* precursors at stage 1, which then declined by stage 2 (Figure 5a). This expression pattern suggests that S_{20}-*AlSMI1* and S_{13}-*AlSMI2* might act to suppress *SP11*. Additionally, we analyzed the expression of mature 24-nt S_{20}-*AlSmi1-a* and S_{13}-*AlSmi2* in early stage anthers (stages 1–2) of $S_{20}S_{13}$ heterozygotes via stem-loop RT-qPCR of RNA samples [22] (Figure 5b). The results suggest that the precursors of these sRNAs and mature 24-nt sRNAs are expressed in vivo.
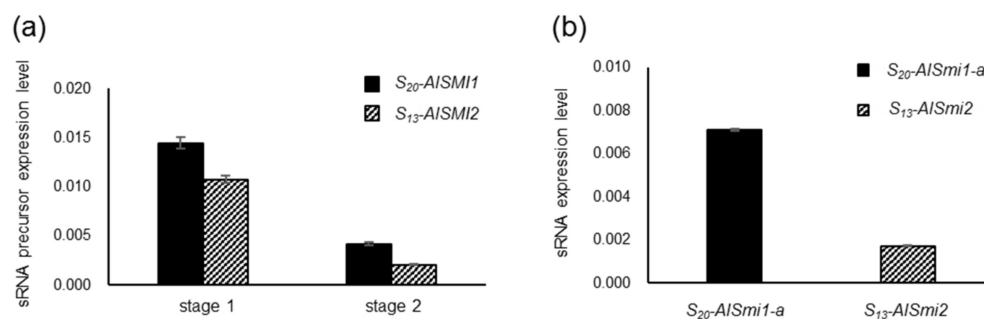
Figure 5. Accumulation of sRNA precursors and a 24-nt sRNA in early stage anthers of $S_{20}S_{13}$ heterozygotes. (**a**) RT-qPCR of S_{13}-*AlSMI2* and S_{20}-*AlSMI1* precursors at stages 1 and 2 in $S_{20}S_{13}$ heterozygotes. *GAPDH* was used as an endogenous reference gene. The results shown are means ± s.d. of 3 replicates. (**b**) Quantification of S_{13}-*AlSmi2* and S_{20}-*AlSmi1* in mixtures of stage 1 and 2 anthers in $S_{20}S_{13}$ heterozygotes via stem-loop RT-PCR analysis. *miR166* was used as an endogenous reference gene. The results shown are means ± s.d. of 3 replicates.

3. Discussion

In this study, we identified two sRNAs homologous to *SP11* genes in *A. lyrata*. The accumulation of the S_{13}-*SP11* transcript in $S_{20}S_{13}$ heterozygotes was strongly suppressed (to approximately 1%) compared with that in $S_{13}S_{13}$ homozygotes (Figure 1b), suggesting that class-IV S_{20}-*SP11* is dominant over class-III S_{13}-*SP11*. *AlSmi1-a* from class IV is thought to be the only sRNA that controls the relationship class IV > (class III, class II, class I) (Figure 2a–e). Class-II and class-III *AlSMI1* gene sequences with polymorphisms are also conserved (Supplementary Figure S1). Class II-specific *AlSmi1-b* shares high similarity with a relatively recessive S_1-*SP11* (class I) exon junction (mispair score 3.0) (Figure 3a–d; Supplementary Figure S1 and S2), suggesting that sRNA processed from this region might be involved in the dominance relationship between class-II and class-I sRNAs (class II > class I). Another sRNA, *AlSmi2*, which shares high similarity with *SP11* genes of relatively recessive *S* haplotypes, is involved in the dominance relationship class III > (class II, class I) (Figure 4a–e). The accumulation of both S_{20}-*AlSMI1* and S_{13}-*AlSMI2* precursors was detected (Figure 5a), and mature 24-nt sRNAs of S_{20}-*AlSmi1-a* and S_{13}-*AlSmi2* were expressed in vivo (Figure 5b). These results suggest that the linear dominance hierarchy in *A. lyrata* is controlled by two polymorphic sRNAs, *AlSmi1* and *AlSmi2* (Figure 6).
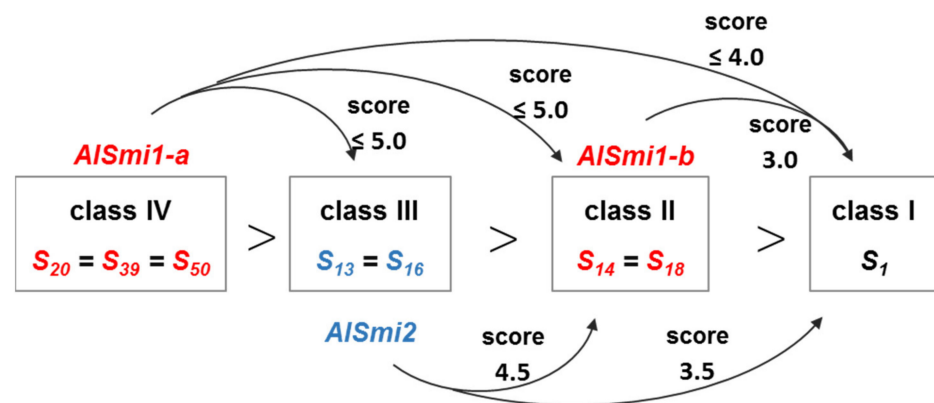
Figure 6. Regulatory network of the identified sRNAs and their predicted targets in *A. lyrata.* Class-IV S_{20}-*SP11* is dominant over class-III S_{13}-*SP11* (Figure 1). *AlSmi1-a* from class-IV *S* haplotypes is homologous to *SP11* from recessive *S* haplotypes (classes III, II, and I), showing a mispair score < 5.0 (Figure 2). *AlSmi1-b* predicted from class-II *S* haplotypes is homologous to a class-I *SP11*, showing a mispair score < 3.0 (Figure 3). *AlSmi2* from class-III *S* haplotypes is homologous to *SP11* from relatively recessive *S* haplotypes (classes II and I), showing a mispair score < 4.5 (Figure 4). Both precursors and mature 24-nt sRNA of *AlSmi1-a* and *AlSmi2* were detected in vivo (Figure 5).

AlSmi1 and *AlSmi2* correspond to *mirS3* and *mir1887* in *A. halleri*, respectively [9]. A species-wide survey of sequence diversity revealed that a large fraction of alleles at the pistil side SI determinant *SRK* are trans-specifically shared between *A. lyrata* and *A. halleri* [23]. Our findings suggest that not only *SRK* but also other *S*-locus genes, including sRNAs, are shared between *A. lyrata* and *A. halleri.* These sRNAs are conserved in both species in the regulation of pollen side dominance. A pollen side linear dominance hierarchy controlled by sRNAs has also been identified in *B. rapa* [11,12], pointing to a common sRNA-based dominance–recessivity mechanism in Brassicaceae plants.

Furthermore, our data suggest that the dominance–recessivity mechanism in both *B. rapa* and *A. lyrata* is explained by the sequence homology between sRNA and its target. In our previous report, the sRNA from the dominant allele had a mispair score < 5.5 against the target region of recessive *SP11*. In the current study, *AlSmi1* and *AlSmi2* in *A. lyrata* also had mispair scores < 5.0 against relatively recessive *SP11s* (Figures 2e, 3d, 4e and 6; Supplementary Figure S2). Concurrently, these sRNAs had a mispair score > 6.5 against self- and relatively dominant *SP11s* (Figures 2e, 3d and 4e; Supplementary Figure S2). Two models have been examined in *A. halleri*: (1) dominant *S* alleles carry a larger set of sRNAs; and (2) recessive *S* alleles carry a larger set of sRNA targets [9]. Here, we identified only one sRNA, *AlSmi1-a,* from the most dominant *S* haplotype (class IV), and found that recessive *S* haplotypes did not contain a larger number of sRNA targets (Figures 2b, 3c and 4d). These results strongly suggest that the polymorphic dominance modifier model we proposed for *B. rapa* also explains the dominance relationships in *A. lyrata*. Further analysis of the role of the interactions between sRNAs and their target regions should provide support for this model.

Similar complex dominance–recessivity relationships can be observed in other SI plants of the Asteraceae and Convolvulaceae [24,25]. Moreover, dominance relationships have been reported among mimicry genes in butterflies [26] and among genes in various plants and animals [27–30]. Further studies are needed to determine whether our model can explain these complicated dominance–recessivity networks and monoallelic gene expression.

4. Materials and Methods

4.1. Plant Materials

A. lyrata SaSb seeds were a gift from Y. Takada (Tohoku University). For all experiments, floral buds from clonally propagated progenies of a single individual were used. The plants were grown in a growth chamber under long-day conditions (16 h light/8 h dark).

4.2. RT-qPCR of SP11

Total RNA was isolated from the anthers of $S_{13}S_{13}$ homozygotes and $S_{20}S_{13}$ heterozygotes at each stage of development and used for RT-qPCR, as previously described [13]. The S_{13}-*SP11* region was amplified using specific primers: forward primer, 5'-AGCCATGTTCAA GGAATGGAAGA-3'; reverse primer, 5'-TTGTTGCCATCCTCCGTAAGGTC-3'. *Elf1α* was used as an endogenous reference gene and amplified using specific primers: forward primer, 5'-TGGTGACGCTGGTATGGTTA-3'; reverse primer, 5'-GGTCTGCCTCATGTCCC TAA-3'.

4.3. Prediction of Inverted Repeat Sequence Regions

Inverted repeat sequences were searched from the *S*-locus sequence data of each haplotype: S_{20} (HQ379628), S_{39} (KJ772415–KJ772419), S_{50} (HQ379631), S_{13} (ADBK01001387), S_{16} (HQ379629), S_{14} (KJ772405–KJ772407), S_{18} (KJ772408–KJ772414), and S_1 (KJ772401–KJ772404). The *S* locus was defined as the region between *PUB8* (*At4g21350*) and *ARK3* (*At4g21380*), as described previously [15]. First, each *SP11* gene containing both upstream and downstream 500-bp fragments was divided into 500-bp fragments overlapping every 30-bp region. These fragments were used as queries in BLAST searches against the *S* loci of the S_{20} and S_{13} haplotypes. Sequences showing *E*-values $< 1 \times 10^{-3}$ were further analyzed. The secondary structures of the precursors from the obtained inverted repeat were predicted using RNAfold [20]. Hairpin-structured miRNA-like sequences having low energy values under -30 kcal mol^{-1} were screened.

4.4. Small RNA Sequencing and Mapping

Total RNA containing the sRNA fraction was isolated from a mixture of stage 1 and 2 anthers using a *mir*Vana miRNA Isolation Kit (Ambion/Thermo Fisher Scientific, Waltham, MA, USA). Preparation of the small RNA library, Illumina GAII sequencing, and adaptor trimming of sequencing reads were performed at Hokkaido System Science Co., Ltd (Sapporo, Japan). sRNA sequences with more than 10 reads were mapped against the *S* locus of the S_{20} haplotype (HQ379628) and the S_{13} haplotype (ADBK01001387). We also mapped the obtained reads against the predicted precursors of *AlSMI1* and *AlSMI2* using the *Bowtie* program [31]. The mispair score was calculated as described [21]: mismatches were scored as 1, and G:U pairs were scored as 0.5. Mismatched and G:U pair scores within the core segment were doubled.

4.5. RT-qPCR of sRNA Precursor

Total RNA was isolated from anthers of $S_{20}S_{13}$ heterozygotes at each stage of development using an RNeasy Mini Kit (QIAGEN GmbH, Hilden, Germany) and used for RT-qPCR, as previously described [13]. Each sRNA precursor region was amplified using specific primers: S_{20}-*AlSMI1* forward primer, 5'-AGCAATGGTTTCAGATTTTGACAGTAACC-3'; S_{20}-*AlSMI1* reverse primer, 5'-AGATACATTTTACCTTGAACATGGTTTAAATGG-3'; S_{13}-*AlSMI2* forward primer, 5'-TTAATTAAAAGTAACTTGTTCACTTAGATTGTTCTTAG-3'; S_{13}-*AlSMI2* reverse primer, 5'-ATGTTGTTCTCTTAGACTCTACTTAGTACG-3'. *GAPDH* was used as an endogenous reference gene and amplified using specific primers: forward primer, 5'-GACCTTACTGTCAGACTCGAG-3'; reverse primer, 5'-CGGTGTATCCAAGGAT TCCCT-3'.

4.6. Stem-Loop RT-PCR

Quantification of 24-nt S_{20}-*AlSmi1* and S_{13}-*AlSmi2* sRNAs was performed as previously described [22]. sRNAs were isolated from anthers (mixture of stages 1 and 2) from $S_{20}S_{13}$ heterozygotes using a *mir*Vana miRNA Isolation Kit (Ambion/Thermo Fisher Scientific, Waltham, MA, USA) and reverse transcribed using a TaqMan MicroRNA Reverse Transcription Kit (Applied Biosystems/Thermo Fisher Scientific, Waltham, MA, USA) with 24-nt sRNA-specific RT primers: S_{20}-*AlSmi1* RT-forward primer, 5'-GTTGGCTCTGGTGCAGGGT CCGAGGTATTCGCACCAGA-3'; S_{13}-*AlSmi2* RT-forward primer, 5'-GTTGGCTCTGGTGC AGGGTCCGAGGTATTCGCACCAGA-3'. The reverse transcription products were quantified using Light Cycler 480 Probes Master Mix (Roche, Basel, Switzerland) and Universal Probe Library #21 (Roche) with small RNA-specific primers and universal primers: S_{20}-*AlSmi1* forward primer, 5'-CGGCGGCAATCAAAACTTAAAGGAG-3'; S_{13}-*AlSmi2* forward primer, 5'-CGGCGGCCACTTAGATTGTTCTTAG-3'; universal primer, 5'-GTGCAGG GTCCGAGGT-3'. *miR166* was used as an endogenous reference miRNA and was amplified using specific primers: RT-forward primer, 5'-GTTGGCTCTGGTGCAGGGTCCGAGGTAT TCGCACCAGAGCCAACGGGGAA-3'; forward primer, 5'-CAGCATCGGACCAGGCTT CA-3'.

References

1. Suzuki, G.; Kai, N.; Hirose, T.; Fukui, K.; Nishio, T.; Takayama, S.; Isogai, A.; Watanabe, M.; Hinata, K. Genomic organization of the *S* locus: Identification and characterization of genes in *SLG/SRK* region of S^9 haplotype of *Brassica campestris* (syn. rapa). *Genetics* **1999**, *153*, 391–400. [CrossRef]
2. Schopfer, C.R.; Nasrallah, M.E.; Nasrallah, J.B. The male determinant of self-incompatibility in *Brassica*. *Science* **1999**, *286*, 1697–1700. [CrossRef]
3. Takayama, S.; Shiba, H.; Iwano, M.; Shimosato, H.; Che, F.S.; Kai, N.; Watanabe, M.; Suzuki, G.; Hinata, K.; Isogai, A. The pollen determinant of self-incompatibility in *Brassica campestris*. *Proc. Natl. Acad. Sci. USA* **2000**, *97*, 1920–1925. [CrossRef]
4. Stein, J.C.; Howlett, B.; Boyes, D.C.; Nasrallah, M.E.; Nasrallah, J.B. Molecular cloning of a putative receptor protein kinase gene encoded at the self-incompatibility locus of *Brassica oleracea*. *Proc. Natl. Acad. Sci. USA* **1991**, *88*, 8816–8820. [CrossRef]
5. Takasaki, T.; Hatakeyama, K.; Suzuki, G.; Watanabe, M.; Isogai, A.; Hinata, K. The *S* receptor kinase determines self-incompatibility in *Brassica* stigma. *Nature* **2000**, *403*, 913–916. [CrossRef]
6. Kachroo, A.; Schopfer, C.R.; Nasrallah, M.E.; Nasrallah, J.B. Allele-specific receptor-ligand interactions in *Brassica* self-incompatibility. *Science* **2001**, *293*, 1824–1826. [CrossRef]
7. Takayama, S.; Shimosato, H.; Shiba, H.; Funato, M.; Che, F.S.; Watanabe, M.; Iwano, M.; Isogai, A. Direct ligand-receptor complex interaction controls *Brassica* self-incompatibility. *Nature* **2001**, *413*, 534–538. [CrossRef]
8. Kusaba, M.; Dwyer, K.; Hendershot, J.; Vrebalov, J.; Nasrallah, J.B.; Nasrallah, M.E. Self-incompatibility in the genus Arabidopsis: Characterization of the *S* locus in the outcrossing *A. lyrata* and its autogamous relative *A. thaliana*. *Plant Cell.* **2001**, *13*, 627–644. [CrossRef]

9. Durand, E.; Méheust, R.; Soucaze, M.; Goubet, P.M.; Gallina, S.; Poux, C.; Fobis-Loisy, I.; Guillon, E.; Gaude, T.; Sarazin, A.; et al. Dominance hierarchy arising from the evolution of a complex small RNA regulatory network. *Science* **2014**, *346*, 1200–1205. [CrossRef]

10. Hatakeyama, K.; Watanabe, M.; Takasaki, T.; Ojima, K.; Hinata, K. Dominance relationships between *S*-alleles in self-incompatible *Brassica campestris* L. *Heredity* **1998**, *80*, 241–247. [CrossRef]

11. Tarutani, Y.; Shiba, H.; Iwano, M.; Kakizaki, T.; Suzuki, G.; Watanabe, M.; Isogai, A.; Takayama, S. *Trans*-acting small RNA determines dominance relationships in *Brassica* self-incompatibility. *Nature* **2010**, *466*, 983–986. [CrossRef] [PubMed]

12. Yasuda, S.; Wada, Y.; Kakizaki, T.; Tarutani, Y.; Miura-Uno, E.; Murase, K.; Fujii, S.; Hioki, T.; Shimoda, T.; Takada, Y.; et al. A complex dominance hierarchy is controlled by polymorphism of small RNAs and their targets. *Nat. Plants* **2016**, *3*, 16206. [CrossRef]

13. Shiba, H.; Kakizaki, T.; Iwano, M.; Tarutani, Y.; Watanabe, M.; Isogai, A.; Takayama, S. Dominance relationships between self-incompatibility alleles controlled by DNA methylation. *Nat. Genet.* **2006**, *38*, 297–299. [CrossRef]

14. Prigoda, N.L.; Nassuth, A.; Mable, B.K. Phenotypic and genotypic expression of self-incompatibility haplotypes in *Arabidopsis lyrata* suggests unique origin of alleles in different dominance classes. *Mol. Biol. Evol.* **2005**, *22*, 1609–1620. [CrossRef] [PubMed]

15. Guo, Y.L.; Zhao, X.; Lanz, C.; Weigel, D. Evolution of the *S*-locus region in Arabidopsis relatives. *Plant Physiol.* **2011**, *157*, 937–946. [CrossRef] [PubMed]

16. Goubet, P.M.; Bergès, H.; Bellec, A.; Prat, E.; Helmstetter, N.; Mangenot, S.; Gallina, S.; Holl, A.C.; Fobis-Loisy, I.; Vekemans, X.; et al. Contrasted patterns of molecular evolution in dominant and recessive self-incompatibility haplotypes in *Arabidopsis*. *PLoS Genet.* **2012**, *8*, e1002495. [CrossRef] [PubMed]

17. Schierup, M.H.; Mable, B.K.; Awadalla, P.; Charlesworth, D. Identification and characterization of a polymorphic receptor kinase gene linked to the self-incompatibility locus of *Arabidopsis lyrata*. *Genetics* **2001**, *158*, 387–399. [CrossRef]

18. Mable, B.K.; Beland, J.; Di Berardo, C. Inheritance and dominance of self-incompatibility alleles in polyploid *Arabidopsis lyrata*. *Heredity* **2004**, *93*, 476–486. [CrossRef]

19. Kusaba, M.; Tung, C.W.; Nasrallah, M.E.; Nasrallah, J.B. Monoallelic expression and dominance interactions in anthers of self-incompatible *Arabidopsis lyrata*. *Plant Physiol.* **2002**, *128*, 17–20. [CrossRef]

20. Lorenz, R.; Bernhart, S.H.; Höner zu Siederdissen, C.; Tafer, H.; Flamm, C.; Stadler, P.F.; Hofacker, I.L. ViennaRNA package 2.0. *Algorithms Mol. Biol.* **2011**, *6*, 26–39. [CrossRef]

21. Fahlgren, N.; Carrington, J.C. miRNA target prediction in plants. *Methods Mol. Biol.* **2010**, *592*, 51–57. [CrossRef] [PubMed]

22. Chen, C.; Ridzon, D.A.; Broomer, A.J.; Zhou, Z.; Lee, D.H.; Nguyen, J.T.; Barbisin, M.; Xu, N.L.; Mahuvakar, V.R.; Andersen, M.R.; et al. Real-time quantification of microRNAs by stem–loop RT–PCR. *Nucleic Acids Res.* **2005**, *33*, e179. [CrossRef]

23. Castric, V.; Bechsgaard, J.; Schierup, M.H.; Vekemans, X. Repeated Adaptive introgression at a gene under multiallelic balancing selection. *PLoS Genet.* **2008**, *4*, e1000168. [CrossRef]

24. Kowyama, Y.; Takahasi, H.; Muraoka, K.; Tani, T.; Hara, K.; Shiotani, I. Number, frequency and dominance relationships of *S*-alleles in diploid *Ipomoea trifida*. *Heredity* **1994**, *73*, 275–283. [CrossRef]

25. Brennan, A.C.; Tabah, D.A.; Harris, S.A.; Hiscock, S.J. Sporophytic self-incompatibility in *Senecio squalidus* (Asteraceae): *S* allele dominance interactions and modifiers of cross-compatibility and selfing rates. *Heredity* **2011**, *106*, 113–123. [CrossRef] [PubMed]

26. Joron, M.; Papa, R.; Beltrán, M.; Chamberlain, N.; Mavárez, J.; Baxter, S.; Abanto, M.; Bermingham, E.; Humphray, S.J.; Rogers, J.; et al. A conserved supergene locus controls colour pattern diversity in *Heliconius* butterflies. *PLoS Biol.* **2006**, *4*, e303. [CrossRef]

27. Guo, M.; Rupe, M.A.; Zinselmeier, C.; Habben, J.; Bowen, B.A.; Smith, O.S. Allelic variation of gene expression in maize hybrids. *Plant Cell* **2004**, *16*, 1707–1716. [CrossRef]

28. Gimelbrant, A.; Hutchinson, J.N.; Thompson, B.R.; Chess, A. Widespread monoallelic expression on human autosomes. *Science* **2007**, *318*, 1136–1140. [CrossRef]

29. Zhuang, Y.; Adams, K.L. Extensive allelic variation in gene expression in populus F$_1$ hybrids. *Genetics* **2007**, *177*, 1987–1996. [CrossRef]

30. Wang, J.; Valo, Z.; Smith, D.; Singer-Sam, J. Monoallelic expression of multiple genes in the CNS. *PLoS ONE* **2007**, *2*, e1293. [CrossRef]

31. Langmead, B.; Trapnell, C.; Pop, M.; Salzberg, S.L. Ultrafast and memory-efficient alignment of short DNA sequences to the human genome. *Genome Biol.* **2009**, *10*, R25. [CrossRef] [PubMed]